NANO LETTERS

2006
Vol. 6, No. 4
626−632

Synchronous Electrorotation of Nanowires in Fluid

Brian Edwards,[†] Theresa S. Mayer,[‡,§] and Rustom B. Bhiladvala*[,‡,§]

Pennsylvania State University, 104 Davey Laboratory, University Park, Pennsylvania 16802

Received November 11, 2005

ABSTRACT

We demonstrate electrorotation of metal nanowires phase-locked to a driving alternating current electric field. Field rotation was accomplished by a low-frequency signal that modulates the amplitude of the high-frequency field. Steady, synchronous rotation of the nanowires was observed for frequencies up to a maximum rotational frequency, which depends on the magnitude of the applied electric field. A locally two-dimensional nanowire fluid flow model was developed to calculate the viscous fluid drag torque, including drag contributions due to the proximity of the floor. Synchronicity and phase-lock angle predicted by equating the calculated fluid drag and electrical driving torques is in good agreement with experimentally determined values, which provides support for the model. Synchronous electrorotation allows for precise control of nanowire rotational speed and orientation for frequencies as low as a fraction of 1 Hz. Potential applications include reconfigurable polarization filters, microfluidic valves, and stirring devices.

The motion of individual nanometer and micrometer-scale particles in fluid can involve a complex balance between competing electrical,[1,2] magnetic,[3] chemical,[4−6] particle-inertia, viscous,[2] gravitational,[2] and Brownian[2,7] forces. The ability to model these interactions for predicting particle movement would enable fundamental studies of colloidal behavior[2,8] as well as new nanoparticle-directed assembly[9,10] methods and microfluidic control strategies. For example, reconfigurable polarization filters[11] and optoelectronic light valves[7] could be fabricated from arrays of metal nanowires whose angular rotational speed and orientation can be controlled using externally applied fields. Controlling individual particles in this manner would also have potential application in lab-on-a-chip systems[12] to serve as microfluidic valves and localized fluid stirring devices.

Asynchronous electrorotation (AER) has been studied previously to differentiate biological cells based on variations in electrical permittivity[13,14] and more recently to drive rotary motion of metal nanowires.[15] In AER, an electrical dipole is induced on the particle by a high-frequency rotating electric field that is produced by applying signals with 90° phase difference to pairs of orthogonally oriented electrodes; frequencies exceeding 1 kHz are typically required to overcome screening of the dipole by mobile ions present in fluids of interest (e.g., water, buffer). Particle rotation is observed as the field-induced dipole experiences a torque tending to align it with respect to the electric field vector that rotates at the high frequency of the applied signal.[16] For most particles and fluids of interest, viscous drag forces prevent the particles from rotating at such high frequencies.[1,16,17] Thus, the rotational speed of the particle is determined by a competition between the driving electrical and resisting fluid torques acting on the particle and can only be changed by varying the magnitude of the applied field.

In this Letter, we report on the first experimental demonstration of *synchronous electrorotation* (SER) using metal nanowires, which are made to spin transversely about their midpoint, *phase locked* to the rotating electric field that drives them. Here, the driving signal is comprised of two independent frequencies. A low-frequency signal modulates the amplitude of the signal that creates the high-frequency field required for particle polarization. In contrast to AER, we show that the rotation frequency of the particle is locked to the low frequency of the modulating signal. Consequently, particle rotation speed is independent of the high-frequency signal, the fluid or particle properties, or the electric field magnitude. Steady, phase-locked rotation continues until a maximum rotational frequency is reached when the nanowires lose synchronization with the rotating field; this occurs when the driving electrical torque is no longer sufficient to overcome fluid drag. We propose a simplified model of the viscous fluid drag torque based on linearity of the equations governing the fluid flow to describe our SER experiment. Synchronicity and phase-lock angle predicted by equating the calculated fluid drag and electrical driving torques are

* Corresponding author. E-mail: rbb16@psu.edu.
[†] Currently at: Department of Electrical and Systems Engineering, University of Pennsylvania, Philadelphia, PA 19104.
[‡] Department of Electrical Engineering, Penn State University.
[§] Materials Research Institute, Penn State University.

10.1021/nl0522328 CCC: $33.50
Published on Web 03/21/2006

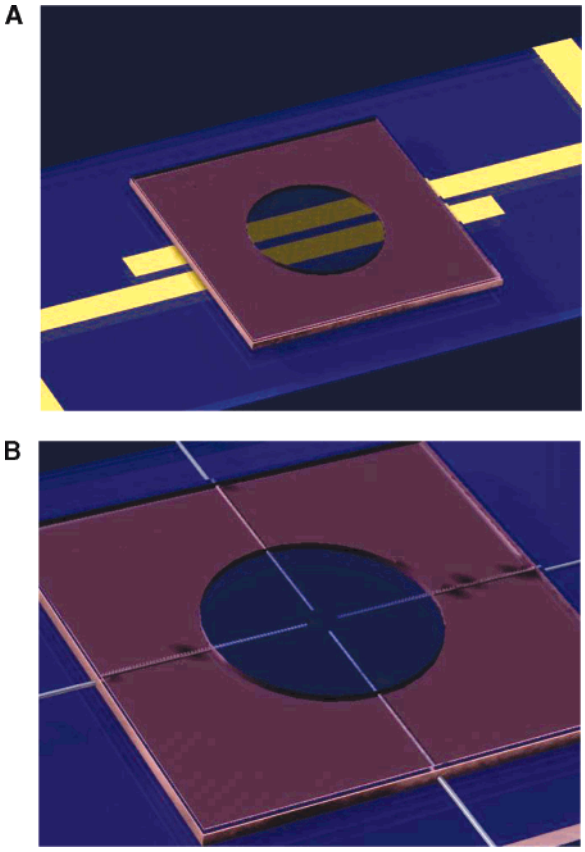

Figure 1. Rendering of microscope slide with a nanorod suspension sealed by a silicone spacer between the slide and a coverslip: (A) two planar electrodes fabricated on a glass slide are used to determine minimum carrier frequency f_c; (B) four pins serve as electrodes for synchronous electrorotation.

in good agreement with experimentally determined values, which lend support to this model. The properties of SER observed here allow for precise control of nanowire rotational speed and orientation at frequencies as low as a fraction of 1 Hz.

The nanowires used in our experiments were synthesized by electrodepositing Au metal segments within the pores of commercially available anodic alumina membranes using established techniques.[18] Following synthesis, nanowires with average length l of 6 μm and radius r of 150 nm were released from the membrane by selective etching and placed in deionized (DI) water, which served as the suspending fluid. A self-assembled monolayer of mercaptoethylsulfonic acid (MESA) was deposited on the surface of the Au nanowires to minimize particle aggregation during SER.[19]

The SER experiments were performed by sealing the nanowire suspension between a glass substrate and a cover slip using a 1 mm thick silicone spacer as shown in Figure 1. The motion of the nanowires was recorded using an optical microscope with an objective lens (20×, NA = 0.45) having a 1.4 μm depth of field. Brownian motion of the nanowires was observed before the external electric field was applied, which ensured that the nanowires were not bound to the substrate floor and were able to move freely during the experiment. Moreover, the nanowires and substrate floor were both in focus using this objective lens, indicating that the nanowires had settled to within 1.4 μm of the substrate floor. The distance separating the nanowires from the substrate floor represents the equilibrium height where gravitational forces are balanced by electrical forces between the negatively charged surfaces of the MESA-coated nanowires and the glass. In modeling SER, we focus on forces and torques in the plane of rotation, which is nominally parallel to the floor. We take the floor-normal force-height equilibrium to be independent of the in-plane forces.

The slowly rotating electric field can be characterized by three parameters: magnitude (E_0), high frequency of the carrier signal (f_c), and low frequency of the modulating signal (f_r). An initial experiment without rotation ($f_r = 0$) was conducted using a pair of coplanar electrodes (see Figure 1A) to determine the minimum value of f_c required to orient the nanowires in the direction of the applied electric field. A bias of 20 V peak-to-peak (V_{p-p}) was applied across the electrodes spaced 800 μm apart, giving $E_0 = 125$ V/cm. Under these conditions, alignment of the nanowires was first observed at $f_c \approx 500$ Hz. A value of $f_c = 1$ kHz was selected for SER experiments to achieve strong alignment of the nanowires in the field direction.

The SER experiments were conducted using two pairs of orthogonally oriented pin electrodes as shown in Figure 1B. This electrode configuration was used for two reasons. First, the orthogonally oriented pairs of pin electrodes provide independent control of the electric field along the x and y axes, with a uniform field in a region near the center of the electrodes. Second, the small cross section of the pins minimizes capacitive effects between adjacent electrodes. Modulating the carrier signal by a factor $\cos(\phi + n(\pi/2))$, where n takes on values 0, 1, 2, and 3 for each of the four electrodes, produces an electric field that oscillates at frequency f_c along a line through the center point of the four pin tips ($x = 0$, $y = 0$) at an angle ϕ with respect to the first electrode. When the angle ϕ is varied as $2\pi f_r t$, the linearly oscillating field is made to rotate at the modulation frequency, f_r (Supporting Information).

The spatial distribution of the equipotential and electric field lines for this electrode configuration was obtained by numerical simulation[21] (Supporting Information), and the resulting equipotential distribution is plotted at equal time intervals spanning a total of 90° of wire rotation, in the left-hand panels of Figure 2. These simulations and all SER experiments were done by applying a modulated carrier signal with $f_c = 1$ kHz and $V_{p-p} = 24$ V across pairs of electrodes separated at their tips by 1300 μm. The field at the center of the four pin tips ($x = 0$, $y = 0$) can be expressed (Supporting Information) as

$$E_{x0} = E_x(\{0,0\}) = E_0 \sin(2\pi f_c t) \cos(\phi)$$

$$E_{y0} = E_y(\{0,0\}) = E_0 \sin(2\pi f_c t) \sin(\phi)$$

$$\phi = -2\pi f_r(t)t \qquad (1)$$

Under these conditions, the electric field is uniform at ($x = 0$, $y = 0$) with $E_0 = 72$ V/cm. In addition, the simulations

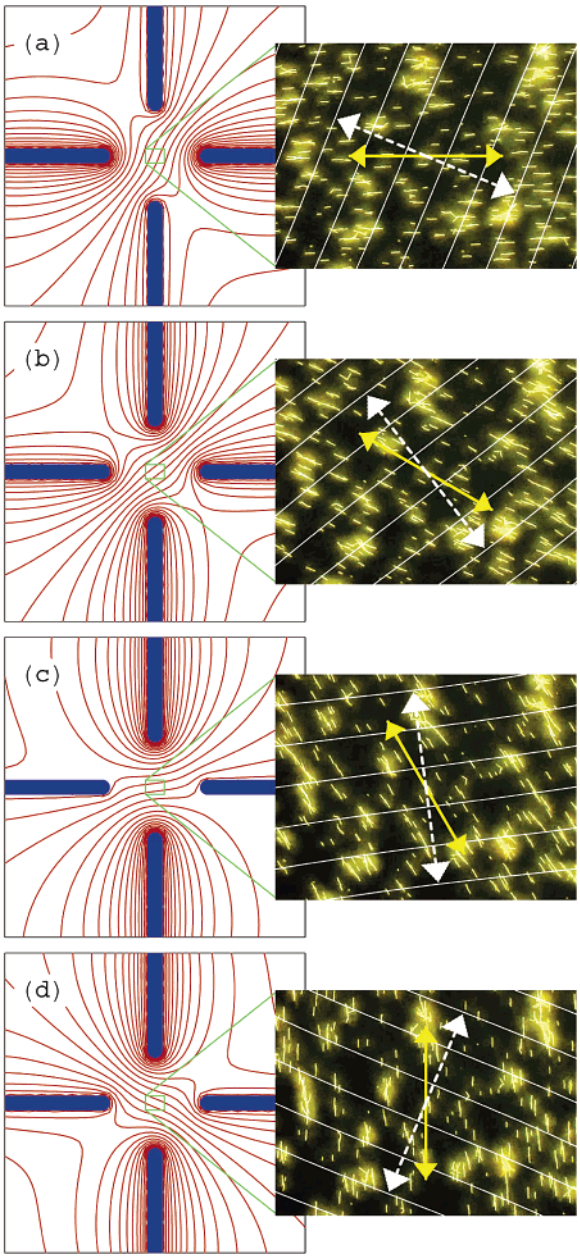

Figure 2. Optical micrographs of the orientation of gold nanowires captured in four steps (a−d), spanning 90° of electric field rotation. Dashed white arrows on micrographs show electric field direction and solid yellow arrows, wire orientation. Associated equipotential lines from electric field simulations at left, indicate the small area spanned by the micrographs, with uniform field, as per eq 2. Opposing electrode tips are 1300 μm apart; vertical edge length of the micrographs is 187 μm.

show that the field uniformity is given by

$$|\vec{E}(\{x,y\}) - \vec{E}(\{0,0\})|/|\vec{E}(\{0,0\})| < 0.1 \qquad (2)$$

in the 200 μm diameter region around (0, 0). Thus, our observation of nanowire motion for SER studies was restricted to this region of the substrate to ensure good field uniformity.

Before introduction of the modulating signal, the carrier signal with $f_c = 1$ kHz and $V_{p-p} = 24$ V was applied across one pair of electrodes and then abruptly switched to the other pair of electrodes. The axes of the nanowires aligned immediately in the direction of the electric field upon energizing the first pair of electrodes. The nanowires then rotated to align with field produced by the second pair of electrodes after the signal was switched. This verified that the as-fabricated electrode structure, E_0, and f_c were suitable for SER experiments.

To investigate SER of nanowires, the modulation frequency f_r was increased linearly from 0 to 2 Hz over a time span of 2.4 min. Four optical micrographs collected at equal time intervals as the electric field rotated through a total of 90° are shown in the right-hand panels of Figure 2. As can be seen from these micrographs, the long axes of the nanowires (solid line) also rotated by 90°. Over this short time, the phase-lock angle, which is the nanowire lag angle θ with respect to the rotating electric field vector (dashed line), remains constant. We measure nanowire angle variation over the entire time of the experiment to check synchronicity, which is defined by a linear wire angular frequency increase with time at the same set rate as the increase of the field rotation frequency. Focusing on individual nanowires in the SER video clip (Supporting Information) showed that the rotational speed increased with f_r until a maximum rotational frequency $f_{r,max}$ was reached, when the nanowires began to drop out of synchronization with the rotating field. This occurred at times of 55−65 s., which corresponds to $f_{r,max}$ of 0.76−0.90 Hz. This small variation can be explained by the distribution of nanowire sizes present in the suspension. For frequencies exceeding $f_{r,max}$, the nanowires stopped rotating and began to flutter as the electric field vector passed through their orientation. An additional data run, with the camera triggered once per field rotation at a fixed field angle, was used to compare lag angle θ from the experiment with results of the SER model developed below, in which the variation of θ with f_r can be explicitly calculated from electric field amplitude, nanowire geometry, and suspending fluid properties. Validation of this model will allow quantitative force−motion predictions for SER using different nanowires and fluids.

We use simplifying assumptions to model the fluid flow and compare estimates of the resistive fluid torque and driving electrical torque on the nanowire. The total resistive fluid drag torque on a rotating cylindrical wire near a floor (see Figure 3) can be obtained by summing the fluid drag forces that are tangential (skin friction) to the cylindrical surface, and the pressure forces that are normal to the surface, over the cylinder. In general, this requires a solution of the nonlinear Navier−Stokes equations for this three-dimensional fluid flow problem that seems analytically intractable in its entirety. Here, we show that several simplifications can reduce the full fluid flow problem to one that allows use of analytical results from simpler flows. In particular, we present arguments to show that the flow past any small length segment of the rotating nanowire may be considered to depend only on the local wire velocity and use this to develop a model for the fluid drag torque.

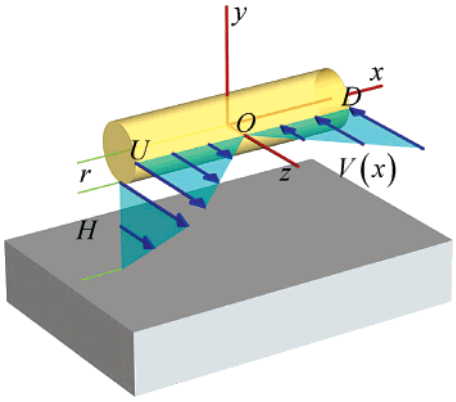

Figure 3. Schematic of rotating nanowire model flow. Profile in the horizontal plane shows velocity of points along the wire length; vertical plane shows fluid velocity distribution between nanowire and floor.

Our modeling begins by determining the relevant Reynolds number (*Re*), equal to the ratio of the fluid inertia force (nonlinear term in the Navier−Stokes equations governing the fluid flow) to the viscous force. For nanowires of radius R, moving through fluid at a steady relative velocity V, $Re = (2\rho VR)/\mu \cong 3 \times 10^{-6}$, where ρ and μ are the density and dynamic viscosity of the fluid, respectively. A value of $Re \ll 1$ indicates that the nonlinear term is negligible, so that the linear, creeping flow (Stokes) equations govern this flow.

The absence of nonlinearities due to the low Reynolds number enables three arguments to justify the use of a locally two-dimensional flow model as discussed below. First, linearity of the governing equations allows us to consider the shear flow between the nanowire and floor and the flow around the nanowire independently and to superpose their results. Second, linearity implies that flow three-dimensionality created by rotation and stretching of vortex lines (see Batchelor[22] for complete discussion of this effect of nonlinearity) is negligible. The third argument involves possible deviations from local two-dimensionality due to pressure variation along the length of the nanowires. This pressure variation can be expected from the upstream high-pressure face (OU in Figure 3) of one-half-length of the nanowire being in line with the downstream low-pressure face (OD of the other half-length) as the nanowire rotates. For any small length segment dl, if the force due to pressure difference between the upstream and downstream faces ($\sim\rho V^2 R\, \mathrm{d}l$) is significant compared to the force due to shear stress ($\sim\mu V\, \mathrm{d}l$), the induced flow along the nanowire length, past the center of rotation will reduce the pressure difference and hence the drag. A locally two-dimensional model that ignores this flow could significantly overpredict the drag torque in this case. Noting that the ratio of the pressure to shear forces varies as ($\rho VR/\mu$), i.e., the Reynolds number, $Re \ll 1$ in our SER experiments, we conclude that the deviation from local two dimensionality is weak and we will neglect it in our analysis.

Assuming a locally two-dimensional flow, the viscous drag on a nanowire of finite length L and radius R, moving at a steady velocity V, can be approximated by the low Reynolds number solution for a prolate spheroid with aspect ratio ≫1 given by[23]

$$F = \frac{4\pi\mu VL}{\ln\left(\frac{L}{R}\right) + \frac{1}{2}} \tag{3}$$

The resisting fluid torque T_{DR} due to steady rotation, neglecting the proximity to the floor, can be estimated using a lumped approximation to calculate the force on each half-length of the nanowire. Since the nanowire is rotating at its midsection about an axis perpendicular to its own (see Figure 3), the velocity of any length segment along the nanowire varies linearly with axial distance from its center. In addition, the drag force given by eq 3 varies linearly with velocity. For a nanowire of total length l, the representative velocity and force for each half-length of the nanowire must be determined at an axial distance of $l/4$ from the center of rotation. Considering each half of the wire, and using eq 3 with $L = l/2$, $R = r$, and $V = 2\pi f_r l/4$, the resisting fluid drag torque T_{DR} due to steady rotation is given by

$$T_{DR} = f_r(\mu l^3)\frac{\pi^2}{2\left\{\ln\left(\frac{l}{2r}\right) + \frac{1}{2}\right\}} \tag{4}$$

The additional torque T_{DF} due to viscous drag from the wire-floor shear layer can be approximated by considering the skin friction due to Couette flow on two plates, each of length $l/2$ and width $2r$ moving parallel to the floor and at a height H above it. Using V defined above to obtain the floor-normal gradient of velocity, we determine that the shear stress is ($\mu 2\pi frl/4H$), which gives an additional drag torque contribution

$$T_{DF} \cong f_r(\mu l^3)\frac{\pi r}{4H} \tag{5}$$

Combining eq 4 and eq 5 gives the total resistive fluid drag torque that accounts for the increase in torque due to floor proximity

$$T_D \cong f_r(\mu l^3)\left[\frac{\pi^2}{2\left(\ln\left(\frac{l}{2r}\right) + \frac{1}{2}\right)} + \frac{\pi r}{4H}\right] = f_r C_{TD} \tag{6}$$

For our calculations, we take H to be approximately equal to the sum of electrical double layer thicknesses adjacent to the substrate floor and nanowire surfaces. Using an equilibrium H^+ ion concentration for carbon dioxide dissolved in pure water of 2.5×10^{-6} M,[22] we estimate $H \approx 220$ nm. In eq 6, the first term in brackets varies slowly and is comparable to 1 for typical values of nanowire aspect ratio ($l/2r$) ranging from 4 to 30. The additional fluid drag torque due to floor proximity (T_{DF}) would thus be significant unless $r/H \ll 1$. T_{DF} is found to be approximately 25% of the total drag torque T_D for the nanowires used here. Using a dynamic

viscosity $\mu = 8.9 \times 10^{-4}$ Pa s, nanowire $l = 6 \times 10^{-6}$ m, $r = 150 \times 10^{-9}$ m, we estimate $C_{TD} = 3.8 \times 10^{-19}$ N m s.

The driving alignment torque on a nanowire due to the rotating electric field can be determined by modeling the nanowire as an infinitely conductive prolate spheroid with major and minor radii of $l/2$ and r, respectively. We assume that the field-induced dipole forms across the long axis of the nanowire, which is oriented at an angle θ with respect to the electric field vector. Thus, the portion of the electric field that intersects the nanowire axis is $E_0 \cos(\theta)$. This gives an induced dipole moment p that can be expressed as $\alpha_{wire} E_0 \cos(\theta)$, where α_{wire} is the nanowire polarizability. Following the treatment described elsewhere,[24] α_{wire} is given by

$$\alpha_{wire} = \frac{4lr^2e^3\pi\epsilon_m}{3(e^2-1)\left(2e - \ln\left(\frac{1+e}{1-e}\right)\right)} \tag{7}$$

where the eccentricity e is defined as

$$e = \sqrt{1 - \frac{r^2}{(l/2)^2}} \tag{8}$$

and ϵ_m is the dielectric permittivity of the suspending fluid.

The magnitude of the electrical alignment torque T_A follows as

$$T_A = |\vec{p} \times \vec{E}| = (\alpha_{rod} E_0 \cos(\theta)) E_0 \sin(\theta)$$
$$= \left(\frac{1}{2}\alpha_{wire} {E_0}^2\right) \sin(2\theta) = C_{TA} \sin(2\theta) \tag{9}$$

This general expression for T_A can be checked for consistency with the known large aspect ratio result.[25] To do so, we set $(2r/l)^2 \ll 1$ in eq 8, retain only the first term in the expansion for e, substitute into eq 7, and rearrange to recover the exact expression for large aspect ratio in a standard reference for electrorotation.[25] Using $E_{0,RMS} = 0.707E_0$, we obtain $C_{TA} = 3.87 \times 10^{-19}$ N·m.

For a nanowire rotating at a steady angular speed, the fluid drag torque must balance the driving electrical torque. Equating T_D from eq 4 to T_A from eq 9 yields

$$f_r C_{TD} = C_{TA} \sin(2\theta) \tag{10}$$

Both C_{TA} and C_{TD} in eq 10 are constant for a given nanowire size, suspending fluid, and field amplitude E_0. Thus, the alignment torque required to maintain steady rotation at any frequency f_r can only increase with f_r through an increase in the angle θ between the induced dipole and the electric field vector. This behavior can be understood by rearranging eq 10 as

$$\theta = \frac{1}{2}\arcsin\left(f_r \frac{C_{TD}}{C_{TA}}\right) \tag{11}$$

The alignment torque reaches its maximum value at $\theta = 45°$. Equating torques for this value of θ, and solving for the maximum rotational frequency $f_{r,max}$ at which the nanowires can be driven yields

$$f_{r,\,max} = \frac{C_{TA}}{C_{TD}} \tag{12}$$

For a given fluid, nanowire size, and floor height, C_{TD} is fixed. Thus, as can be seen from eq 9 and eq 12, higher maximum rotational frequencies ($\sim {E_0}^2$) can be achieved by increasing the electric field amplitude.

We now compare results from our model with the values obtained from our experiments using a linearly increasing electric field rotation frequency. The nanowire angle variation with time, over more than 20 rotations, plotted in Figure 4a, is well described by the best-fit second-order polynomial. The local slope of this polynomial, the wire angular frequency, is plotted in the inset of Figure 4a and shows a linear increase with time, as required by synchronicity, with a maximum frequency of 0.78 Hz before loss of synchronicity. Observed values from several nanowires of slightly different dimensions in the experiment were found to range from 0.76 to 0.90 Hz for this value of E_0. Using the values of C_{TD} and C_{TA} determined previously for a nanowire radius of 0.15 μm and length of 6 μm, the model gives $f_{r,max} = 1.03$ Hz. As seen in Figure 4b, the measured lag angle θ follows the inverse sine curve (eqs 11 and 12) within the estimated $\pm 5°$ angle measurement error shown by the error bars, up to about 80% of the maximum achievable frequency. Beyond this frequency, half of the data points closely follow the curve while the rest show drops in lag angle slightly larger than the angle measurement error. This may be indicative of intermittent loss of synchronicity approaching the limit $f_{r,max}$ and points to the difficulty of accurately locating the limit experimentally. The overall level of agreement between experiments and synchronicity predictions lends support to future predictive use of this simplified model for a difficult fluid flow problem.

The importance of this fluid flow problem is underscored in related studies of colloidal behavior of fiber suspensions and AER of nanowires. Dimensional analysis can be used to show that the fluid drag torque varies with rotation frequency, dynamic viscosity, and nanowire length as ($f_r \mu l^3$), but the exact form of the prefactor involving nondimensional ratios of wire length l, radius r, and height H above floor must be obtained from the solution to a three-dimensional fluid flow problem. Our model (eq 6) provides an approximation to the prefactor with a dependence on r/H and an inverse logarithmic dependence on l/r for the effect of nanowire rotation in bulk fluid. More importantly, it indicates that for typically encountered r, H values in tenths of a micrometer, the contribution from the shear layer between floor and nanowire is significant. In earlier related theoretical work considering fiber suspensions,[26] slender-body theory was invoked to develop a torque result with a similar inverse logarithmic dependence, which yields a slightly higher torque estimate compared to T_{DR} (eq 5) from our model. The floor

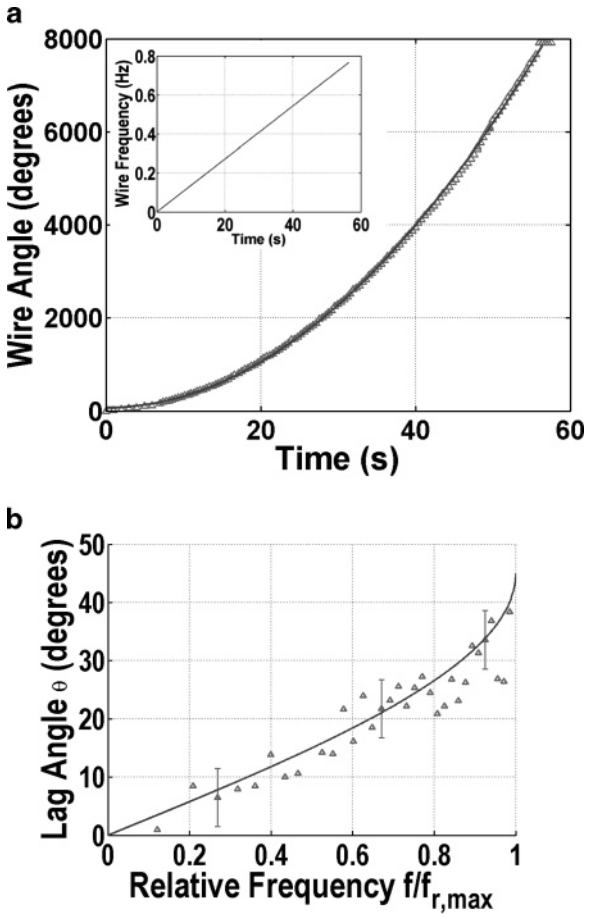

Figure 4. (a) Variation with time of the nanowire angle (triangles) measured from video frames. The data are well described by the best-fit second-order polynomial, shown by the solid line, with local slope (inset), or nanowire rotation frequency, increasing linearly with time at the same rate as the applied field, providing the first measure of overall rotation synchronicity. (b) The lag angle θ between nanowire and field, measured by triggering the camera once per field rotation at the same field angle and plotted against relative frequency, follows the inverse sine relationship, eqs 11 and 12, derived for synchronous rotation. In the steeper region of the inverse sine curve ($f/f_{r,max} > 0.8$), approaching the synchronicity limit, about half the data points follow the curve, while half show drops in the lag angle slightly larger than estimated angle resolution error bars. This is suggestive of intermittent loss of synchronicity approaching the limit $f_{r,max}$ and points to the difficulty in experimental evaluation of $f_{r,max}$.

proximity was not considered because it was not physically relevant to that problem. A recent experimental study[15] of AER determines the best fit to their data to present a prefactor that is given by a third-order polynomial in nanowire length l, independent of nanowire radius r and height H above the floor. With both r and H being smaller than the wavelength of commonly available laser sources, the interferometric determination of height H poses a challenging experimental problem with potential to contribute further to the model presented here.

Comparing SER to AER for steadiness of rotation, we note from recent AER experiments[15] that nanowire motion typically involves tens of milliseconds/rotation with the rotating electric field vector passing the nanowire many times in one nanowire rotation. Viscous diffusion of generated shear leads to acceleration/deceleration (starting/stopping) times $\approx l^2/4\nu$ (ν is the kinematic viscosity), in the approximate range of 2−25 μs for nanowires with length l in the range of 3−10 μm in water. Thus AER for elongated particles such as nanowires typically involves unsteady rotation in which the nanowire experiences rotary "kick-starts" and stops as the electric field rotates past the nanowire axis many times per wire rotation; torque−speed relations must thus be understood as averages of an unsteady process over measurement times. Steady rotation using AER is possible if the time interval between kicks is made smaller than the viscous diffusion time, but this provides a constraint on the choice of carrier frequency. SER provides steady rotation that is phase-locked to the electric field.

To understand the scope of applications of SER and AER, it is useful to consider two sets of nanowires, each having wires of the same size, initially randomly oriented in suspension. SER will cause the two sets to rotate at the same selected frequency but with a fixed relative orientation between them. This creates order not achievable in conventional AER, where the speeds will differ based on nanowire size, while the relative orientation will remain random. However, in AER, individual wire speeds are determined by their drag torque and respond sensitively to nanowire size and fluid properties. Hence, while AER has proven to be an effective tool for differentiating objects using a size or permittivity dependent rotational frequency,[13] SER is better suited to applications which require ordered alignment, for example, assembly of reconfigurable polarization filters. SER, with set steady motion and a validated torque-rotation model, can serve as an experimental testbed for parametric force−motion studies of individual particles and their aggregate behavior in colloidal suspension.[8] For some applications such as microscale fluid stirring, either SER or AER may be used. These examples show that the two methods should be seen as complementary rather than competing techniques.

In summary, we have demonstrated SER of metal nanowires at a steady rotational speed. This speed is fixed by the low frequency f_r of a signal that modulates the amplitude of the signal producing an electric field with high frequency f_c, required for particle polarization. A numerical value of the rotational speed f_r of the particles can be explicitly set, independent of nanowire geometry, fluid properties, electric field magnitude, and frequency f_c. This removes a constraint on f_c, which can be chosen to ensure polarization for a range of values of nanowire aspect ratio, electrical conductivity, and permittivity of the fluid. Rotation remains synchronous with the driving electric field until a maximum rotational speed $f_{r,max}$ is reached. $f_{r,max}$ ($\sim E_0^2$) may be set by choosing the electric field amplitude. Floor proximity correction for fluid drag torque was predicted to be significant, using a tractable analytical model for the three-dimensional fluid flow around the nanowire. A balance between estimates of this drag torque and the electrical driving torque for a given field amplitude yields numerical values for $f_{r,max}$. Overall synchronicity and the values for lag angle calculated from the model are in accord with experimental measurements,

indicating that this flow model may allow quantitative torque-rotation predictions for SER with different types of nanowires and fluids. SER allows for precise control of nanowire rotational speed and orientation at frequencies as low as a fraction of 1 Hz. The properties of SER observed here should enable its use in a range of applications, such as reconfigurable polarization filters, microfluidic valves, and stirring devices.

Acknowledgment. B.E. was supported by NSF MRSEC, Center for Nanoscale Science, Grant No. DMR-0213623. Partial support was provided by NSF NIRT Grant No. ECS-0303981 and CCF-0303976. R.B.B. also acknowledges funding from the Penn State Materials Research Institute, the Huck Institute for Life Sciences, and Tobacco Settlement Funds from the Pennsylvania Department of Health, which specifically disclaims responsibility for any analyses, interpretations, or conclusions. We thank Drs. Ganesh Subramanian, Thomas Mallouk, Paul Lammert, and Vincent Crespi for helpful discussions and for comments on the paper.

Supporting Information Available: A video clip showing SER of Au nanowires, the amplitude modulation scheme for synchronous field rotation, and notes on numerical simulation. This material is available free of charge via the Internet at http://pubs.acs.org.

References

(1) Jones, T. B., *Electromechanics of particles*; Cambridge University Press: Cambridge, 1995.
(2) Russel, W. B.; Saville, D. A.; Schowalter, W. R. *Colloidal Dispersions*; Cambridge University Press: Cambridge, 1989; p 14.
(3) Tanase, M.; Bauer, L. A.; Hultgren, A.; Silevitch, D. M.; Sun, L.; Reich, D. H.; Searson, P. C.; Meyer, G. J. *Nano Lett.* **2001**, *1*, 155.
(4) Soong, R. K.; Bachand, G. D.; Neves, H. P.; Olkhovets, A. G.; Craighead, H. G.; Montemagno, C. D. *Science* **2000**, *290*, 1555.
(5) Pantaloni, D.; Le Clainche, C.; Carlier, M. F. *Science* **2001**, *292*, 1502.
(6) Paxton, W. F.; Kistler, K. C.; Olmeda, C. C.; Sen, A.; St. Angelo, S. K.; Cao, Y.; Mallouk, T. E.; Lammert, P. E.; Crespi, V. H. *J. Am. Chem. Soc.* **2004**, *126*, 13424.
(7) Hsu, H.-Y.; Sharma, N.; Ruoff, R. S.; Patankar, N. A. *Nanotechnology* **2005**, *16*, 312.
(8) Huang, J. P.; Yu, K. W.; Gu, G. Q.; Karttunen, G. Q. *Phys. Rev. E* **2003**, *67*, 051405.
(9) Smith, P. A.; Nordquist, C. D.; Jackson, T. N.; Mayer, T. S.; Martin, B. R.; Mbindyo, J.; Mallouk, T. E. *Appl. Phys. Lett.* **2000**, *77*, 1399.
(10) Hughes, M. P. *Nanotechnology* **2000**, *11*, 124.
(11) Jeong, D. H.; Zhang, Y. X.; Moskovits, M. *J. Phys. Chem. B* **2004**, *108*, 12724.
(12) Stone, H. A.; Stroock, A. D.; Ajdari, A. *Annu. Rev. Fluid Mech.* **2004**, *36*, 381.
(13) Becker, F. F.; Wang, X. B.; Huang, Y.; Pethig, R.; Vykoukal, J.; Gascoyne, P. R. *Proc. Natl. Acad. Sci. U.S.A.* **1995**, *92*, 860.
(14) Wang, X. B.; Huang, Y.; Gascoyne, P. R. C.; Becker, F. F.; Holzel, R.; Pethig, R. *Biochim. Biophys. Acta* **1994**, *1193*, 330.
(15) Fan, D. L.; Zhu, F. Q.; Cammarata, R. C.; Chien, C. L. *Phys. Rev. Lett.* **2005**, *94*, 247208.
(16) Hughes, M. P. *Nanotechnology* **2002**, *13*, 157.
(17) Hagedorn, R.; Fuhr, G.; Muller, T.; Schnelle, T.; Schnakenberg, U.; Wagner, B. *J. Electrost.* **1994**, *33*, 159.
(18) Martin, B. R.; Dermody, D. J.; Reiss, B. D.; Fang, M. M.; Lyon, L. A.; Natan, M. J.; Mallouk, T. E. *Adv. Mater.* (*Weinheim, Ger.*) **1999**, *11*, 1021.
(19) Martin, B. R.; St Angelo, S. K.; Mallouk, T. E. *Adv. Funct. Mater.* **2002**, *12*, 759.
(20) Schwartz, A. T.; Bunce, D. M.; Silberman, R. G.; Stanitski, C. L.; Stratton, W. J.; Zipp, A. P. *Chemistry in Context*; WCB/McGraw-Hill: New York, 1997; p 197.
(21) Brown, R. C.; Hemingway, M. A. *J. Electrost.* **2001**, *53*, 235.
(22) Batchelor, G. K. *An Introduction to Fluid Dynamics*; Cambridge University Press: Cambridge; New York, 1967; pp 266−268.
(23) Sherman, F. S. *Viscous Flow*; McGraw-Hill: New York, 1990; pp 273−279.
(24) Sihvola, A. H. *Electromagnetic mixing formulas and applications*; Institution of Electrical Engineers: London, 1999; pp 63−67.
(25) Jones, T. B. *Electromechanics of particles*; Cambridge University Press: Cambridge, 1995; p 117.
(26) Chen, S. B.; Koch, D. L. *J. Colloid Interface Sci.* **1996**, *180*, 466.

NL0522328